MINERALOGICAL MAGAZINE, MARCH 1982, VOL. 46, PP. 103-110

The mineral chemistry of dolerites and gabbros from the central Complex of Slieve Gullion, NE Ireland

JOHN A. GAMBLE

Department of Geology, Victoria University of Wellington, New Zealand

SYNOPSIS

THE dolerites and gabbros of the Tertiary central complex of Slieve Gullion, NE Ireland, represent a suite of tholeiitic magmas (varying from tholeiitic basalt to tholeiitic andesite, Gamble 1979*a*) which crystallized in the root-zone of a shield volcano. The ubiquity of biotite suggests that the magmas were hydrous and, in addition, both silicate (olivine) and oxide (Ti-magnetite) phases show evidence for oxidation at high temperatures.

The chemistry of the ferromagnesian minerals (olivine, pyroxene, biotite) and plagioclase feldspars behaves in a fashion which is in keeping with the tholeiitic affinity of the suite. In the ferromagnesian minerals moderate iron enrichment accompanies increasing differentiation whilst the plagioclase feldspars display strong compositional zoning indicative of fluctuating P-T conditions during crystallization.

The pyroxenes in some texturally complex dolerites and gabbos show several generations of growth accompanied by subsolidus exsolution. These complex textures have been linked to complications in the crystallization history caused by the coexistence of cooler, volatile-rich granitic magma (Gamble 1979*b*).

The available field evidence (vent agglomerates and lava flows marginal to the encompassing ring-dyke complex, Emeleus, 1962, together with widespread explosive interaction between granitic and basaltic magmas in the central complex, Gamble, 1979*b*) suggests a shallow level of emplacement for the Central Complex magmas. When considered in conjunction with nominal calculations relating to the amount of cover removed since 58 my B.P. (best estimated age for Slieve Gullion from Evans *et al.*, 1973; MacIntyre, 1973) it is unlikely that P_{tot} exceeded 2 kb, more likely 1 kb. Calculations of temperature and f_{O_2} based on coexisting mineral equilibria yield a range of values consistent with the fluctuating conditions under which the mineral assemblages crystallized and equilibriated. Provided that the assumptions necessitated by the dynamic conditions under which the magmas equilibriated are fully realized, it would appear that the basic magmas of the Slieve Gullion Central Complex crystallized about 1050-1100 °C under moderately high oxygen fugacity.

REFERENCES

Emeleus, C. H. (1962) *Proc. R. Ir. Acad.* (B) **62,** 55-76.

Evans, A. L., Fitch, F. J., and Miller, J. A. (1973) *Q. J. Geol. Soc. London*, **129,** 419-43.

Gamble, J. A. (1979*a*) *Contrib. Mineral Petrol.* **69,** 5-19.

——(1979*b*) *J. Volc. Geotherm. Res.* **5,** 297-316.

MacIntyre, R. M. (1973) In *Geochronology and Isotope Geology of Scotland. Field Guide and Reference*, K1-25.

[*Manuscript received 27 January 1981; revised 6 May 1981*]

© *Copyright the Mineralogical Society*

THE MINERAL CHEMISTRY OF DOLERITE AND GABBROS FROM THE CENTRAL COMPLEX OF SLIEVE GULLION, NORTH EAST IRELAND.

J.A. Gamble

Department of Geology, Victoria University of Wellington, New Zealand.

INTRODUCTION

The igneous central complexes of the British Tertiary volcanic province mark the sites of deeply denuded shield volcanoes. The Slieve Gullion complex, northeast Ireland, consists of two structural units, an early ring-dyke complex of felsite and granophyre (Richey & Thomas, 1932; Emeleus, 1962) which encompasses a later central complex composed principally of dolerites and gabbros, microgranites and granophyres. (Richey, 1935; Reynolds, 1951; Bailey & McCallien, 1956; Gamble, 1979a). In the central complex these granitic and basaltic magmas were emplaced,sometimes contemporaneously, to form a series of sub-horizontal sheet-like structures. The structural relationship of these intrusions are discussed in Gamble (1979a).

Chemically, the basaltic rocks vary from olivine tholeiite to tholeiitic andesite and define a low pressure fractionation sequence controlled by crystallisation of plagioclase and olivine (Gamble, 1979a). Mineralogical evidence of the tholeiitic character is provided by the coexisting Ca-rich and Ca-poor pyroxenes and an ilmenite-spinel opaque assemblage. The ubiquity of biotite indicates that the rocks crystallised in the presence of a volatile phase. Textural variations have been attributed to the interaction between hot basaltic liquids or rocks and low density, volatile-rich granitic magmas (Gamble, 1979b).

This paper presents chemical data for minerals from a suite of analysed (Gamble, 1979a)dolerites and gabbros from the central complex. The data are evaluated, in conjunction with field observations, in an attempt to constrain the P-T conditions under which the magmas crystallised.

TEXTURAL VARIATIONS

Modal analyses of specimens analysed by the electron microprobe are contained in Table 1. In addition, details of specimen localities and short petrographic notes relating to chemically analysed material have been presented in an appendix to Gamble (1979a). The majority of specimens investigated in this study are non-porphyritic (specimen 72/45 carries phenocryst olivine and specimens 72/31, AT70 and AT1490 contain sparse phenocrysts of plagioclase). Nevertheless, the variations in texture and grain-size not only throughout the suite, but often within the area of a single thin section, defy accurate description by the terms dolerite, microgabbro or gabbro, even though the terms have been used in a general sense in the field (see footnote, Gamble, 1979b). In an attempt to overcome this difficulty, an estimate of average grain-size in each specimen is contained in the final column of Table 1. From this data the reader may deduce relative conditions for crystal growth and nucleation.

Specimen Number	AT12	AT24	AT40	AT1410	AT1490	AT70	72/19	72/15	72/21	72/22	72/25	72/24	72/31	72/45
Olivine	-	-	6.33	6.00	0.70	5.13	-	-	-	-	-	-	0.30	15.13
Plagioclase	49.03	61.09	63.41	55.60	60.80	56.60	41.82	46.20	46.34	39.77	51.02	41.90	54.20	39.27
Pyroxene	25.55	16.00	21.78	20.20	21.60	30.39	47.09	30.20	29.53	20.83	29.87	43.80	28.00	22.59
Opaques	0.97	4.80	1.61	3.10	1.30	3.23	9.64	3.60	4.49	4.55	5.19	1.30	1.10	3.42
Biotite	4.42	5.00	0.43	2.20	0.70	1.33	9.64	8.90	6.93	5.68	6.49	3.00	1.90	5.18
Amphibole	14.78	7.40	1.18	3.80	2.00	0.38	0.36	3.60	4.36	5.30	2.97	4.80	2.20	3.42
Quartz	4.60	3.20	-	-	-	0.28	1.09	2.40	0.90	10.89	3.90	1.00	0.30	-
K-Feldspar	-	-	-	-	-	-	-	-	-	6.16	-	-	-	-
Mesostasis	0.80	2.30	5.26	12.30	1.90	2.66	-	5.90	7.45	6.82	0.56	4.20	12.00	10.98
Grain Size (mm)	1.25	3.00	1.50	1.00	2.00	2.00	0.10	1.00	0.50	0.75	0.50	1.25	2.50	0.25

TABLE 1 Modal analyses (in volume %) of analysed dolerites and gabbros from the central complex of Slieve Gullion. Abbreviations: Pyroxene, includes both Ca-rich and Ca-poor pyroxene; Opaques includes ilmenite, magnetite and sulphides. The final line gives a nominal estimate of grain size in mm.

CHEMICAL MINERALOGY OF THE BASIC ROCKS OF SLIEVE GULLION

Analytical Methods

Material for electron microprobe analysis was selected from a suite of chemically analysed specimens (Gamble, 1979a). They were selected in order to portray the mineralogy of a wide range of chemical and textural compositions. Modal analyses of the analysed specimens are presented in Table 1.

Mineral analyses were determined on polished, carbon-coated rock thin sections using a JEOL JXA-50A electron microprobe fitted with an EDAX lithium drifted silicon detector energy dispersive spectrometer. An accelerating voltage of 15KV was used for all analyses and the beam current (generally about 1.5nA) was monitored by means of a Faraday cup on the specimen holder. Counting times of 100 seconds were used, permitting the accumulation of approximately 500,000 counts per analysis. The accumulated spectrum was stored in a multi-channel analyser. Natural minerals and oxides were used as standards. Spectrum stripping and corrections for dead-time, peak-overlap, escape and sum peaks and the Z.A.F. correction were performed by online computer following Reed & Ware (1975). The analyses quoted in Tables 2 to 6 are means of at least five spot analyses. Detection limits of the analytical system are as follows:

Na 0.2%; Mg 0.15%; Al, Si, K, Ca, Ti, V, Cr, Mn, Fe, Ni 0.10%.

Olivine

Representative analyses of olivine are presented in Table 2 and the range of compositions, within individual rock specimens and the suite as a whole, are displayed in figures 1 and 2.

A range between Fo_{56} and Fo_{92} is interrupted by a compositional gap separating high-magnesian olivine phenocrysts (mean core composition, Fo_{89}) from groundmass olivine (range Fo_{77}-Fo_{56}). The high-Mg olivines display both chemical and morphological similarities to olivines from the Rhum layered intrusion (Wager & Brown, 1968; Dunham & Wadsworth, 1978). On the basis of chemical composition and mass balance calculations with enclosing groundmass, Gamble (1979a, p.7-8) concluded that the high-Mg "phenocryst" olivines were xenocrystic and probably elutriated from a deeper seated crustal magma reservoir of Rhum type. On the other hand, the composition of groundmass olivine (Fo_{74}-Fo_{56}) implies that the magmas are fractionated with regard to their mantle source region, Gamble 1979a.

The groundmass olivines yield additional information relating to the conditions under which the magmas equilibrated. Sporadic development of symplectic intergrowths, particularly in the coarser gabbroic specimens (specimens 72/24, AT24, 72/31; see plate 1C), indicate oxidation at high temperatures (Haggerty & Baker, 1967). Electron microprobe analyses of the intergrowth material suggest a reaction of the type:

$$3(Mg,Fe)_2SiO_4 + 3SiO_2 + 4O_2 \rightarrow 3Mg_2Si_2O_6 + 2Fe_3O_4$$

olivine + residual melt → opx + mt

which is consistent with oxidation at a late magmatic stage. Analyses of the products are contained in the Appendix.

Further evidence for high temperature oxidation of olivine is indicated by the presence, in olivine crystals, of oriented dendritic platelets (see Gamble et al., 1976 for photomicrographs). A transmission electron microscope study of similar platelets in olivines from the Rhum intrusion has been carried out by Putnis (1979) who concluded that the platelets are eutectoidal intergrowths of clinopyroxene and magnetite representing products of oxidation at high temperatures. In specimens from Slieve Gullion both dendritic platelets and symplectite intergrowths have been recognised within single olivine crystals. Textural relationships in the grains suggest nucleation of the platelets prior to decomposition of the olivine to symplectite.

Plagioclase

Plagioclase is the principal groundmass and phenocryst phase in the basic rocks of Slieve Gullion, Table 1. In the field certain dolerite layers can be distinguished by an abundance of plagioclase phenocrysts, Reynolds (1951) naming one such horizon as feldspar-phyric dolerite (her layer 4). Further detailed mapping (Gamble, 1975) on the north slopes of Slieve Gullion and a study of drill-core and sub-surface exposures (Gamble et al., 1976) found similar feldspar-phyric dolerite horizons (interstratified with aphyric dolerite) to be relatively common throughout the Lower Dolerite intrusions.

Plagioclase phenocrysts show more complex and pronounced compositional zoning than groundmass crystals. In the latter, normal zoning is commonly developed whereas in phenocryst plagioclase examples of normal, oscillatory and reverse zoning have all been observed. The more complex zoning of the phenocryst plagioclase clearly reflects non-equilibrium conditions during crystallisation.

Table 3 contains representative analyses of plagioclase. The chemical variation (in terms of Ab - Or - An, atomic percent) is given in Figure 3. The most notable chemical features of the plagioclase group are:

1) The highly calcic (up to An_{97}) nature of crystal cores in the more primitive dolerites (e.g. AT40 and 72/41).

2) The extent of zoning shown by all specimens (e.g. AT40, range An_{87} to An_{44}.

3) The very low K_2O content measured in all plagioclase analyses, even at relatively high Ab contents.

	AT70	AT1490	AT1410	72/41	AT40	AT64	72/45
SiO_2	34.27	36.02	37.45	36.87	38.21	40.88	39.18
MnO	0.74	0.57	0.40	0.45	0.31	-	0.25
FeO	36.92	33.96	25.79	28.95	24.03	9.83	17.39
MgO	27.43	29.35	35.94	33.72	37.22	49.29	42.62
CaO	0.08	0.09	-	-	-	-	-
NiO	-	-	-	-	0.22	-	0.49
Total	99.44	99.99	99.58	99.99	99.99	100.00	99.93
Cation formula based on 4 oxygens							
Si	0.965	0.995	0.996	0.993	1.003	1.001	0.965
Mn	0.018	0.013	0.009	0.010	0.007	-	0.005
Fe	0.869	0.785	0.572	0.652	0.527	0.201	0.370
Mg	1.152	1.209	1.421	1.353	1.456	1.798	1.618
Ca	0.003	0.003	0.005	-	-	-	-
Ni	-	-	-	-	0.005	-	0.010
Fo Content (Atomic Percent)	57.0	60.5	71.3	67.5	73.4	89.9	81.4

TABLE 2 Electron microprobe analyses of representative olivines from the central complex of Slieve Gullion. Each analysis is the mean of six spot analyses.

These chemical and zonal features can be readily accounted for by consideration of the bulk chemical composition of the magmas (primitive basaltic melts from the Slieve Gullion complex are rich in calcium, CaO ∿ 11%, and low in potassium, K_2O ∿ 0.2%) and by fluctuations of PH_2O during crystallisation (cf. Johannes, 1978). The consistently low K_2O values clearly reflect the low initial K content of the parent magmas. Enrichment of K in residual (mesostatial) liquids together with an increasing H_2O content eventually led to late crystallisation of biotite and amphibole (K_2O ∿ 8-11%).

Pyroxenes

1) Pyroxene exsolution and textures

Ca-rich and Ca-poor pyroxenes are present in all the rocks investigated in this report. They are found only as groundmass phases and vary in texture from poikilitic and ophitic to granular and intersertal. Ca-rich pyroxene (augite) is more abundant and in many of the coarse gabbros the Ca-poor phase

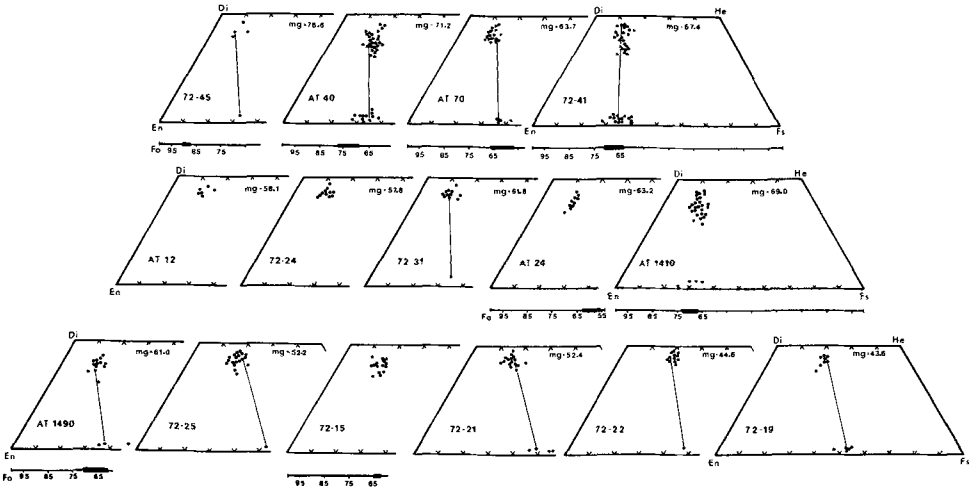

FIGURE 1 Chemical variation in pyroxene and olivine minerals for a selected suite of dolerites and gabbros from the Slieve Gullion Central Complex. Pyroxene analyses are plotted in the conventional En - Fs - Di - He quadrilateral in terms of En - Fs - Wo (Atomic percent). Olivine analyses are expressed in terms of Fo content (Atomic percent). Tie lines join coexisting mineral pairs.

is sparsely developed.

In the Ca-rich pyroxenes exsolution lamellae are difficult to detect by optical means. On the other hand, in the Ca-poor pyroxenes exsolution is manifest and frequently complex. Commonly, grains display the characteristic blebby or graphic exsolution, typical of inverted pigeonite (Deer et al., 1978 and Plate 1E). Interpretation of the cooling history of these grains suggests high temperature (often random) exsolution of augite blebs from pigeonite and subsequent exsolution of augite (often less calcic) from orthopyroxene (parallel to 100) after the grain had cooled below the clinopyroxene-orthopyroxene inversion temperature. Primary hypersthene containing narrow augite exsolution lamellae parallel to (100) has been identified in some rocks.

	AT40(c)	72/41(c)	AT1410(c)	72/25	72/15(c)	72/21(R)	72/22(R)	72/19(R)
SiO_2	47.36	47.30	49.51	54.80	51.67	57.15	61.37	58.76
Al_2O_3	33.04	34.11	32.28	29.28	30.61	26.24	23.98	25.89
FeO	0.43	0.46	0.45	-	0.27	0.61	0.46	0.36
MnO	-	-	-	-	-	0.12	0.12	-
CaO	17.14	15.97	15.68	11.46	14.05	8.79	6.08	8.23
K_2O	0.08	0.08	0.09	0.24	0.14	0.20	0.47	0.27
Na_2O	1.81	1.96	1.99	4.23	3.47	6.62	7.51	6.56
Total	99.86	99.88	100.00	100.01	100.21	99.73	99.99	100.07
				Cation formula based on 8 oxygens				
Si	2.182	2.170	2.260	2.464	2.346	2.579	2.732	2.627
Al	1.794	1.845	1.737	1.552	1.638	1.396	1.258	1.364
Fe	0.017	0.018	0.017	-	0.010	0.023	0.017	0.014
Mn	-	-	-	-	-	0.005	0.005	-
Ca	0.846	0.785	0.767	0.552	0.684	0.425	0.290	0.394
K	0.005	0.005	0.005	0.014	0.008	0.012	0.027	0.015
Na	0.162	0.174	0.176	0.369	0.305	0.579	0.648	0.569
Ab	16.0	18.1	18.5	39.4	30.6	57.1	67.2	58.2
Or	0.5	0.5	0.6	1.5	0.8	1.1	2.8	1.6
An	83.5	81.4	80.9	59.1	68.6	41.8	30.0	40.2

TABLE 3 Electron microprobe analyses of representative plagioclases from the central complex of Slieve Gullion. Suffix (c) indicates core analysis and (R) rim analysis. Each analysis represents the mean of five spot analyses.

The paragenesis of the pyroxene minerals is complicated by the existence of distinct generations of pyroxene within the same rock. Study of pyroxene textures in a number of specimens has indicated marginal overgrowths of pigeonite on ophitic Ca-rich pyroxene crystals. In the same specimens granular or interstertal pigeonite grains display epitaxial overgrowth of augite (Plate 1D and E) whilst primary hypersthene crystals (with narrow augite lamellae parallel to 100) have a sub-ophitic texture and no clear cut textural association with either augite or pigeonite.

2) Pyroxene chemistry

Representative electron microprobe analyses of pyroxenes from the Slieve Gullion gabbros and dolerites are presented in Tables 4 and 5. The chemical variation (in terms of Di - He - En - Fs, atomic percent) in individual specimens is given in Figure 1 and for all rocks in Figure 2.

The Ca-rich pyroxenes, (Table 4), are augites in the classification scheme of Deer et al. (1978) and display a trend of moderate iron enrichment which accompanies decreasing Mg-number in the whole rock. Concomitant with this trend as the Fe content increases the range of Ca decreases resulting in a broadening of the miscibility gap separating Ca-rich and Ca-poor pyroxenes, Figure 2.

In a single rock specimen, calcium content, which may vary by up to 15 atom percent, for a constant Mg/Fe value, accounts for the principal chemical variation. The minor elements Na, Al, Fe^{3+} (calculated from ΣFeO on the basis of 6 oxygens and 4.0 cations, after Papike et al., 1974), Ti and Cr all show relatively low concentrations indicating minimal amounts of the acmite and tschermak molecules, Table 4. Diopside, hedenbergite, enstatite and ferrosilite constitute the principal end-member compositions in keeping with the tholeiitic affinity of the parent magmas, hence analyses are displayed in terms of the conventional pyroxene quadrilateral.

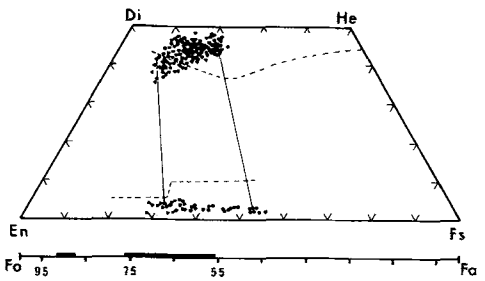

FIGURE 2 Combined chemical variation in pyroxenes and olivines from Slieve Gullion. Data has been screened in order to simplify data presentation and to minimise the effect of Ca-variation due to exsolution. Dashed line shows trend for Skaergaard pyroxenes. Solid lines join coexisting pyroxene pairs in an olivine gabbro and tholeiitic andesite.

The Ca-poor pyroxenes, (Table 5), are pigeonite (now inverted) and hypersthene. When these two minerals coexist in the same rock (e.g. specimens 72/41 and AT40) the hypersthene is more magnesian and lower in Ca and Ti than coexisting pigeonite, (Table 5). The studied specimens reveal a trend of moderate iron enrichment over a compositional range extending from Mg_{71}, Fe_{26}, Ca_3 to Mg_{45}, Fe_{52}, Ca_3. This trend correlates with the decreasing Mg-number in the whole rock and with the trend of the coexisting Ca-rich pyroxenes. Tie-lines are constructed for coexisting pairs. (Note: The tie-lines link crystals which have nucleated and grown in proximity). The projection of these tie-lines intersects the Di - Wo join in the compositional range Wo_{70} - Wo_{80} (Deer et al., 1978).

The coexistence of hypersthene and pigeonite with augite warrants further discussion since the narrow temperature-composition range over which this 3-phase assemblage can crystallise has implications for pyroxene thermometry (see Ross et al., 1973; Ross & Huebner, 1975; Huebner et al., 1975).

Specimens AT40 and 72/41 contain this 3-phase pyroxene assemblage. Pyroxene analyses from these specimens are plotted in the conventional pyroxene quadrilateral in Figures 4 and 5. Textural relationships in these rocks suggest a crystallisation history which follows the sequence illustrated in Figure 6. This diagram indicates plagioclase to be the liquidus phase and with falling temperature it is joined by olivine and then ophitic clinopyroxene (augite). With a further decrease in temperature pigeonite joins augite, often nucleating at the margins of ophitic augite crystals. Cotectic precipitation of augite and pigeonite is indicated by parallel intergrowths between the two phases. Epitaxial overgrowth of augite on inverted pigeonite and crystallisation of hypersthene complete the pyroxene crystallisation.

Specimen Number	AT40	72/41	72/19	AT12	72/24	AT70	72/31	72/15	72/22	72/25
SiO_2	51.95	51.54	50.95	50.81	50.90	51.26	51.04	50.61	51.60	52.42
TiO_2	0.55	0.71	-	0.68	0.53	0.31	0.35	0.74	-	0.30
Al_2O_3	1.89	2.14	1.09	3.42	3.49	3.14	2.63	3.00	0.92	0.72
MnO	0.29	0.29	0.22	0.27	0.22	-	0.24	0.35	0.26	0.38
FeO	10.77	9.82	14.31	8.39	8.01	8.22	9.06	10.63	13.64	12.14
MgO	15.54	15.12	12.08	15.30	15.50	15.76	15.76	15.18	11.34	12.10
CaO	19.68	19.79	21.36	20.81	20.82	21.23	21.14	19.43	22.09	21.59
Na_2O	0.32	0.52	-	-	-	-	-	-	0.62	0.42
Cr_2O_3	-	-	-	0.24	0.38	-	-	0.29	-	0.17
Total	100.99	99.93	100.01	99.92	99.85	99.92	100.22	100.23	100.47	100.24
				Cation formula based on 6 oxygens						
Si_{iv}	1.909	1.912	1.936	1.884	1.885	1.890	1.885	1.882	1.946	1.977
Al_{vi}	0.082	0.088	0.049	0.116	0.116	0.110	0.114	0.118	0.041	0.024
Al	-	0.006	-	0.033	0.037	0.027	-	0.014	-	0.009
Ti	0.015	0.020	-	0.019	0.015	0.009	0.010	0.021	-	0.009
Fe^{3+}	0.087	0.079	0.080	0.038	0.037	0.060	0.097	0.054	0.113	0.024
Mg	0.851	0.836	0.684	0.846	0.856	0.866	0.867	0.841	0.637	0.680
Fe^{2+}	0.244	0.225	0.375	0.222	0.211	0.194	0.183	0.276	0.317	0.359
Mn	0.009	0.009	0.007	0.009	0.007	-	0.008	0.011	0.008	0.012
Ca	0.776	0.787	0.870	0.827	0.826	0.836	0.836	0.774	0.892	0.872
Na	0.023	0.037	-	-	-	-	-	-	0.045	0.031
Cr	-	-	-	0.007	0.011	-	-	0.009	-	0.005
Mg	43.3	43.2	34.0	43.6	44.2	44.2	43.6	43.0	32.4	34.9
ΣFe	17.3	16.2	22.9	13.8	13.2	13.0	14.4	17.5	22.3	20.3
Ca	39.4	40.6	43.1	42.6	42.6	42.8	42.0	39.5	45.3	44.8
				Pyroxene end-member compositions						
ACMITE	0.023	0.037	-	-	-	-	-	-	0.045	0.029
CATIAL206	0.015	0.020	-	0.019	0.015	0.009	0.010	0.021	-	0.009
CAALALS106	0.000	0.006	-	0.033	0.037	0.027	-	0.014	-	0.006
CAFEFES106	0.010	-	0.015	-	-	-	0.001	-	0.014	-
CAFEALS106	0.051	0.042	0.049	0.045	0.048	0.066	0.095	0.063	0.041	-
DIOPSIDE	0.539	0.562	0.517	0.573	0.579	0.603	0.599	0.505	0.556	0.555
HEDENBERGITE	0.156	0.157	0.289	0.156	0.148	0.135	0.132	0.172	0.283	0.303
ENSTATITE	0.156	0.137	0.084	0.136	0.139	0.132	0.134	0.168	0.041	0.063
FERROSILITE	0.046	0.039	0.047	0.037	0.035	0.030	0.030	0.058	0.021	0.034

TABLE 4 Electron microprobe analyses of representative Ca-rich pyroxenes from the central complex of Slieve Gullion. Each analysis represents the mean of at least six spot analyses. End-members calculated after allocating iron Fe^{2+} and Fe^{3+} on the basis of stoichiometry (Papike et al., 1974).

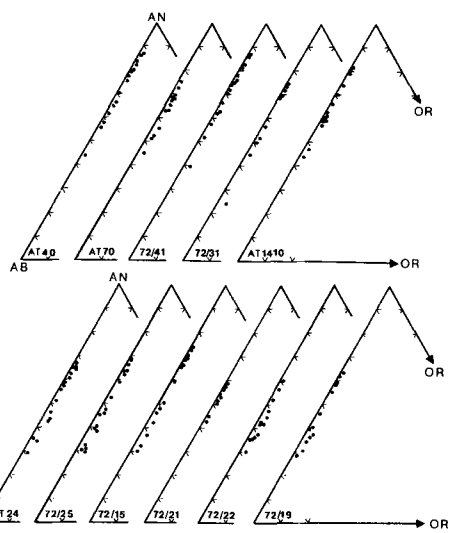

FIGURE 3 Chemical variations in plagioclase feldspars (expressed in terms of atomic percent An - Ab - Or) for a selected suite of dolerites and gabbros from the Slieve Gullion Central Complex.

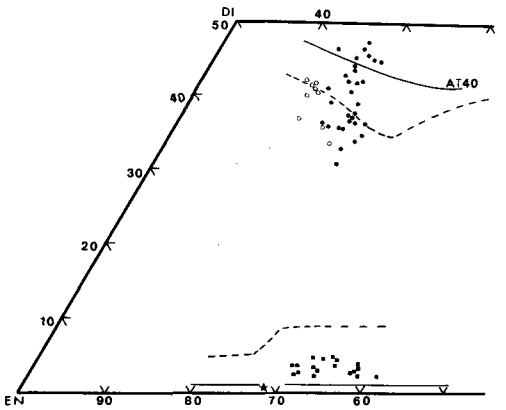

FIGURE 4 Quadrilateral plots of pyroxenes in a single specimen (AT40). Symbols: open circles - ophitic clinopyroxenes; closed circles - granular and epitaxial clinopyroxenes; closed stars - primary hypersthene; closed squares - inverted pigeonite. Solid lines represent subsolidus curves and dashed lines solidus curves for Skaergaard pyroxenes, (Nwe, 1976; Coleman, 1978).

In the pyroxene quadrilateral diagrams (Figures 4 and 5), the range in Ca-content in the granular pyroxenes has resulted from plotting analyses of solidus and subsolidus phases. The Ca-rich granular pyroxenes with high Wo-content are subsolidus augites associated with primary exsolution from pigeonite. They correspond to the sub-solidus trend for Skaergaard pyroxenes demonstrated by Nwe (1976) and Coleman (1978). The Ca-rich granular pyroxenes with lower Wo-content are augites growing parallel to or epitaxially on pigeonite (see Plate 1E, analysis 1). These analyses conform reasonably with the Skaergaard pyroxene solidus curves of Nwe (1976) and Coleman (1978). The scatter of points between the subsolidus and solidus curves reflects the inability of the EPMA system to resolve between fine lamellae and host phases. The early crystallising ophitic augites are more magnesian and approximate to the Skaergaard solidus trend.

The Ca-poor pyroxenes reveal the presence of a phase change from hypersthene to pigeonite (now inverted) between En_{70} and En_{67}. The analyses of hypersthene are restricted in composition while the pigeonites display slight iron

Specimen Number	AT1410(H)	AT1410(P)	AT1490	72/41(H)	72/41(P)	AT40	72/21	72/31	AT70
SiO_2	54.97	53.46	51.01	54.71	53.49	53.08	51.51	52.69	51.07
TiO_2	0.13	0.57	0.29	-	0.25	0.36	0.22	0.14	0.20
Al_2O_3	0.97	0.88	0.43	0.48	0.49	0.82	0.31	0.69	0.92
MnO	0.38	0.51	0.66	0.50	0.58	0.65	0.87	0.64	0.73
FeO	15.99	19.54	28.58	18.36	19.91	21.65	29.21	24.40	25.94
MgO	26.92	23.35	17.03	25.44	22.65	21.25	16.43	20.34	19.93
CaO	0.64	1.68	1.50	0.52	2.65	2.19	1.19	1.10	1.22
Na_2O	-	-	0.50	-	-	-	0.19	-	-
Cr_2O_3	-	-	-	-	-	-	-	-	-
Total	100.00	99.99	100.00	100.01	100.02	100.00	99.93	100.00	100.01
				Cation formula based on 6 oxygens					
Si_{iv}	1.983	1.971	1.973	1.995	1.982	1.980	1.994	1.985	1.947
Al_{vi}	0.017	0.029	0.020	0.005	0.018	0.020	0.006	0.015	0.041
Al	0.024	0.009	-	0.016	0.003	0.016	0.008	0.016	-
Ti	0.004	0.016	0.009	-	0.007	0.010	0.006	0.004	0.006
Mn^{2+}	0.012	0.010	0.022	0.015	0.018	0.020	0.029	0.020	0.024
Fe^{2+}	0.482	0.603	0.924	0.560	0.617	0.676	0.946	0.769	0.827
Mg	1.447	1.283	0.981	1.383	1.251	1.182	0.948	1.142	1.133
Ca	0.025	0.067	0.062	0.020	0.105	0.088	0.049	0.044	0.050
Na	-	-	0.038	-	-	-	0.014	-	-
Cr	-	-	-	-	-	-	-	-	-
Mg	74.1	65.7	49.9	70.4	63.4	60.8	48.79	58.4	56.4
ΣFe	24.7	30.9	47.0	28.6	31.3	34.7	48.67	39.3	41.1
Ca	1.2	3.4	3.1	1.0	5.3	4.5	2.54	2.3	2.5

TABLE 5 Electron microprobe analyses of representative Ca-poor pyroxenes from the central complex of Slieve Gullion. Suffix (H) indicates primary hypersthene, (P) pigeonite, now inverted to orthopyroxene. Each analysis represents the mean of at least six spot analyses.

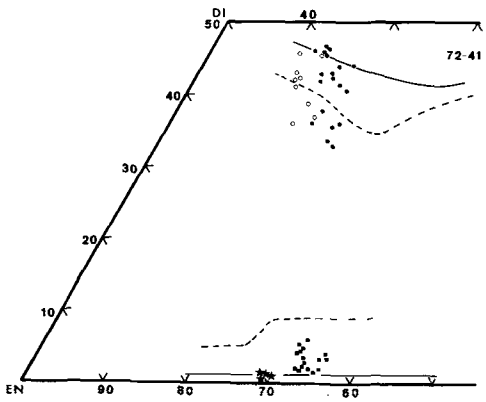

FIGURE 5 Quadrilateral plots of pyroxenes in a single specimen (72/41). Symbols as in Figure 4.

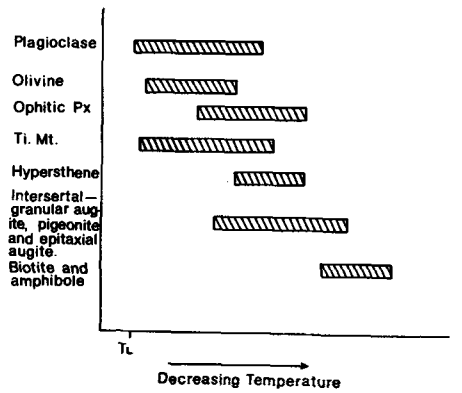

FIGURE 6 Generalised crystallisation relationships in the dolerites and gabbros. T_L indicates liquidus temperature.

enrichment and a range of Wo-content, the latter resulting from the overlap of the beam spot between lamellae and host phases.

The bulk composition of liquids from which these 3 phase assemblages have crystallised range from 100.Mg/Mg+Fe = 67 to 71. Using the experimental data of Ross & Huebner (1975) the crystallisation temperatures can be estimated to lie between 1000°C and 1100°C. However, these temperatures are likely to be maxima since the effects of P_T and P_{H_2O} have not been considered. Temperatures have also been calculated from coexisting Ca-poor pyroxene (hypersthene) - Ca-rich pyroxene (augite) assemblages using the methods of Wood & Banno (1973) and Wells (1977). The temperatures of ^890°C and ^895°C are appreciably lower than those estimated from the Ross-Huebner geothermometer, but, in keeping with the textural relationships, may be realistic as near solidus or subsolidus temperatures (cf. Nobugai et al., 1978 who, using similar methods, estimate temperatures of 985°C, pigeonite-augite, and 881-856°C, subsolidus, for the Skaergaard intrusion).

The influence of P_{H_2O} is probably critical since microscopic exsolution products in the rims of ophitic augite crystals and in granular pigeonites often include a brown amphibole phase (basaltic hornblende) (Plate 1b). Furthermore, crystallisation under conditions of increasing P_{H_2O} (indicated by increases of modal biotite and amphibole with ^Mg-number in the whole rock) may also account for the increasing Wo-content of the Ca-rich pyroxenes in the more fractionated dolerites (Figure 2) by a mechanism similar to that proposed for the pyroxenes in the Kap Edvard Holm Intrusion (Deer & Abbott, 1965; Elsdon, 1971). In this case, the increasing width of the pyroxene solvus would also suggest that the Slieve Gullion pyroxenes crystallised at lower temperatures than comparable pyroxenes from the Skaergaard intrusion.

3) Minor Element Distribution in Clinopyroxenes

In basaltic pillow lavas the minor element chemistry of clinopyroxenes (particularly Al and Ti) has been used to indicate cooling rates (Mevel & Velde, 1976; Coish & Taylor, 1979). Bence & Papike (1972), Grove & Bence (1977) and co-workers have studied pyroxene-liquid relationships in lunar basalts and concluded that partitioning of the minor elements (Al_2O_3, TiO_2 and Cr_2O_3) are strongly dependent on cooling rate and the extent to which crystallisation of plagioclase and ilmenite are suppressed.

This approach was applied to clinopyroxenes in Slieve Gullion rocks which display textures suggestive of a complex crystallisation history. On textural grounds the pyroxenes have been identified as granular, poikilophitic and ophitic varieties, the former being produced by rapid crystallisation and/or larger degrees of undercooling. In Figure 7, the Ti - Al data for granular pyroxenes display a scatter about the 1/4 trend line while ophitic pyroxenes plot beneath this line indicating higher Al content at equivalent Ti.

It is suggested that the higher Al content of the ophitic crystals has resulted from cessation or suppression of plagioclase crystallisation during nucleation and growth of the ophitic pyroxene crystals.

Biotite

Biotite is ubiquitous in dolerites and gabbros from Slieve Gullion, Table 1. Interpretation of textural relationships indicates that it is late to crystallise either forming mesostasis, rimming magnetite and ilmenite grains or less commonly forming marginal intergrowths (with amphibole) to pyroxene crystals. A conspicuous increase of modal biotite in the differentiated dolerites and gabbros (those rocks with 100.Mg/Mg+Fe <60) is paralleled by a tendency for biotite to be more abundant in the gabbroic rocks than in dolerites which display similar Mg-values. A progressive increase in the water content of the magmas and fluctuations of water vapour pressure during crystallisation of the magmas offer plausible explanations for these features.

Representative analyses and mineral formulae are contained in Table 6. In terms of Mg : Fe ratios all the analysed minerals are biotites (sensu stricto) with Mg : Fe<2. 100. Mg/Mg + Fe (Atomic) ranges from 61.6 to 41.7 indicating moderate iron enrichment which is displayed in the plot of Mg - Fe - Al, Figure 8. This moderate iron enrichment trend is accompanied by a slight depletion of Al.

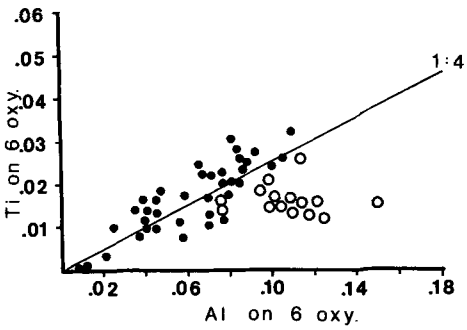

FIGURE 7 Ti/Al relationships for calcium-rich pyroxenes in two dolerite specimens (AT40 and 72/41). Symbols: open circles - ophitic pyroxenes; closed circles - granular and epitaxial pyroxenes.

	AT40	72/31	72/24	72/22	72/25	72/19
SiO_2	36.50	34.07	35.89	35.37	35.70	34.69
TiO_2	4.78	4.59	5.00	4.96	4.39	4.15
Al_2O_3	12.14	14.50	12.52	12.41	12.84	12.71
FeO	22.14	16.54	22.43	22.31	23.63	21.65
MgO	11.30	14.34	10.56	10.74	10.13	11.01
CaO	0.11	0.16	0.20	-	-	-
K_2O	8.71	10.87	9.14	11.63	11.35	11.30
Na_2O	-	-	0.38	-	-	-
Total	95.68	95.07	96.12	97.42	98.04	95.51
	Cation formula based on 24 oxygens					
Si	6.140	5.719	6.051	5.969	6.000	5.956
Ti	0.604	0.579	0.634	0.629	0.555	0.536
Al	2.407	2.868	2.488	2.468	2.543	2.571
Fe	3.114	2.322	3.163	3.149	3.321	3.108
Mg	2.833	3.586	2.654	2.701	2.538	2.817
Ca	0.019	0.029	0.036	-	-	-
K	1.869	2.327	1.966	2.504	2.433	2.474
Na	-	-	0.124	-	-	-

TABLE 6 Electron microprobe analyses of representative biotites from the central complex of Slieve Gullion. Each analysis is the mean of three spot analyses.

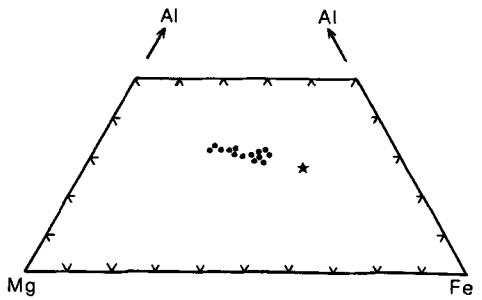

FIGURE 8 Chemical variation in biotites from Slieve Gullion dolerites and gabbros expressed in terms of Mg - Fe - Al (Atomic percent). The star is a biotite from a typical central complex granophyre.

The Opaque Minerals

The opaque minerals include oxide and sulphide phases. The oxides, which are predominant, are magnetite and ilmenite, occur in all rocks and a red-brown chromian spinel occurs as inclusions in xenocrysts of high-Mg olivine and in the groundmass of rocks in which these xenocrysts occur. The chrome spinels are interpreted as liquidus or near-liquidus phases whereas the magnetite and ilmenite display textures suggesting a wide crystallisation interval.

Pyrrhotite, chalcopyrite and pyrite are the principal sulphide phases (in order of decreasing abundance). Pyrrhotite often rims ilmenite or magnetite grains whilst chalcopyrite and pyrite are confined to mesotasis.

The compositions of coexisting magnetite and ilmenite offer an opportunity to estimate equilibration temperatures and oxygen fugacity from coexisting Fe - Ti oxide pairs (Buddington & Lindsley, 1964). However, other workers (e.g. Mathieson, 1975; Bowles, 1977 and Himmelberg & Ford, 1977) have found that the Fe - Ti oxides of intrusive rocks continue to equilibrate at subsolidus temperatures reducing the ulvo-spinel content of recalculated magnetite and resulting in unreliable T-fo_2 estimations. The rocks from Slieve Gullion are no exception and magnetite reveals both coarse granular and lamellae types of ilmenite "exsolution" product.

	Magnetite AT12	Ilmenite AT12		Magnetite AT70	Ilmenite AT70
TiO_2	2.21	48.42		4.49	50.89
SiO_2	0.17	-		0.13	-
FeO	32.91	40.60		35.14	44.60
MgO	-	-		-	1.11
MnO	0.17	2.59		0.23	0.88
CaO	0.22	0.28		0.15	0.22
Fe_2O_3	61.59	6.15		54.91	1.80
Al_2O_3	0.56	-		2.23	-
V_2O_3	1.75	0.95		1.43	0.30
Cr_2O_3	0.37	0.16		0.42	0.19
Total	99.95	99.11		99.15	99.99
Usp (mol.%)	9.64	R_2O_3 (mol.%)	Usp (mol.%)	11.36	R_2O_3 (mol.%)
T°C	600	6.48	T°C	615	1.92
$-\log_{10}fO_2$	20		$-\log_{10}fO_2$	22	

TABLE 7 Electron microprobe analyses of magnetites and ilmenites from the central complex of Slieve Gullion. Analyses carried out using a scanning electron-beam. Fe_2O_3 content estimated from ΣFeO following the procedures of Carmichael (1967).

With electron microprobe analysis this difficulty can be partly offset by analysing with a scanning electron beam but the existence of coarse granular exsolution products of ilmenite from magnetite means that analytical data should be interpreted with caution. The temperature and fo_2 estimations for Slieve Gullion rocks, (Table 7) following the recalculation procedures of Carmichael (1967), are too low to be representative of magmatic temperatures and evidently are related to the widespread development of granule type ilmenite "exsolution" from magnetite. The analyses plotted in Figure 9 demonstrate a scatter which corresponds closely with the QFM. (Quartz-Fayalite-Magnetite) buffer curve. Using a temperature of 1050°C (T°C maximum from pyroxene geothermometry) an oxygen fugacity of c. 10^{-11} bar can be inferred for the Slieve Gullion magmas provided they equilibrated close to the QFM buffer curve.

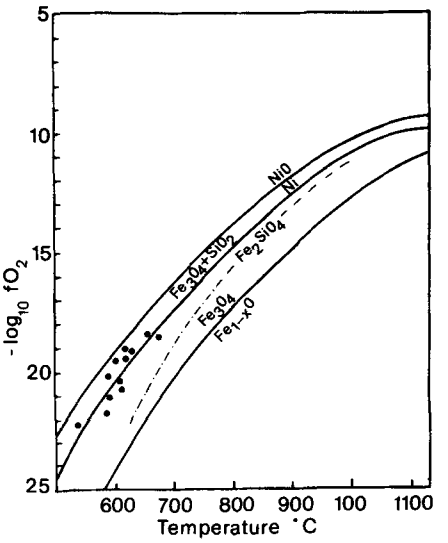

FIGURE 9 Plot of temperature (°C) and $-\log_{10}fo_2$ for Slieve Gullion dolerites and gabbros. Buffer curves are from Buddington & Lindsley (1964). The equilibration curves for the Skaergaard intrusion are from Mathieson (1975). The dashed line is based on Fe - Ti oxide compositions while the dot-dash line represents the inferred behaviour on further cooling.

DISCUSSION

The most primitive magmas emplaced into the root zone of the Slieve Gullion volcano appear to be analogues of the high-calcium, low-alkali tholeiitic liquids which have been recognised on Skye and Rhum (Drever & Johnston, 1966; Thompson et al., 1972; Esson et al., 1975; Gibb, 1976; Mattey et al., 1977; Donaldson, 1977; Thompson et al., 1980). Low pressure (crustal) fractionation of these magmas, principally involving plagioclase and olivine, produced a spectrum of compositions ranging from olivine tholeiite to tholeiitic andesite (Gamble, 1979a). Internal contacts, a lack of mineral layering and the gravity anomaly data of Cook & Murphy (1952) led Gamble (1979a) to propose that the magmas had differentiated prior to emplacement. Fluctuations in P_{H_2O} and temperatures, enhanced by contiguous, cooler, granitic magmas, produced a wide range of textures in the basic rocks (Gamble, 1979a, b).

The mineral chemistry presented in this paper support these observations but permit a more precise assessment of the conditions under which the magmas crystallised. For example, temperature calculations based on pyroxene Fe : Mg exchange equilibria and experimental data yielded temperatures between 1100°C and 890°C. Rock textures and subsolidus exsolution in the pyroxenes suggest that these temperatures reflect suprasolidus and subsolidus conditions. Experimental runs at 1 atmosphere (dry) on similar tholeiites from Skye (Esson et al., 1975) show plagioclase as the liquidus phase (1225°C) with clinopyroxene appearing after a 41°C fall in temperature (1184°C). Using this data, together with the fact that higher P_{H_2O} conditions would lead to depression of the liquidus, temperatures between 1000°C and 1100°C may be reasonable estimates for the Slieve Gullion basic magmas. Temperatures calculated from coexisting Fe - Ti oxide phases yield unrealistic magmatic temperatures, a feature which has been observed in other intrusive suites of tholeiitic composition (Mathieson, 1975; Himmelberg & Ford, 1977). However, by assuming that the assemblage equilibrated close to or just above the QFM buffer and using a temperature of 1050°C (a combination of pyroxene geothermometry plus experimental data), the oxygen fugacity can be estimated to lie between 10^{-10} and 10^{-11}. Comparison with fo_2 estimates from the Skaergaard intrusion (Figure 9, data from Mathieson, 1975) shows that fo_2 was some 10^2 log units higher in the case of the Slieve Gullion. Whilst the method of fo_2 estimation in the case of the Slieve Gullion magmas has been based on a number of assumptions (necessitated by a lack of equilibrium relationships between coexisting mineral assemblages) the values are thought to be realistic since they are supported by several independent lines of evidence. Firstly, the ubiquity of biotite, which increases in modal volume with differentiation and which may indicate progressively increasing P_{H_2O}. Secondly, the evidence for various types of high temperature oxidation in olivine and thirdly, the progressive increase (with decreasing Mg-value) in the miscibility gap separating coexisting Ca-rich and Ca-poor pyroxenes.

Finally, the contemporaneity both in space and time of relatively large volumes of granitic magma should be considered. In view of the probable significance of magma mixing as a triggering mechanism for volcanic eruptions (Anderson, 1976; Sparks et al., 1977; Eichelberger, 1980) we have, at Slieve Gullion, the opportunity to review the situation in the now crystallised contents of a magma chamber. Here, Gamble et al. (1976) and Gamble (1979b) have described a spectrum of contact relationships between contiguous basaltic and granitic magmas, With net-veining, intrusion breccias and hybrid rocks representing the ultimate products of explosive brecciation and magma mixing respectively. Furthermore, many of the textural variations detected in the gabbros and dolerites, even though they were far from granite, could be attributed to processes such as sudden chilling, decompression or volatile transfer which accompanied periods of injection of cooler, volatile-rich granitic magmas. With this in mind it is difficult to escape the conclusion that the contemporaneity of granitic magmas led to sustained high temperature oxidising conditions during and after crystallisation of the basic magmas.

CONCLUSIONS

The petrology and chemical mineralogy of the dolerites and gabbros from the Slieve Gullion central complex are consistent with crystallisation of tholeiitic magma under shallow crustal conditions. The ubiquity of biotite indicates the hydrous condition of the magmas from which the rocks crystallised and the variety of textures (Gamble, 1979b) suggest that the conditions of crystallisation were subject to rapid fluctuations. A continuous variation in the chemistry of the ferromagnesian minerals (olivine, pyroxene and biotite) outlines a trend of limited iron enrichment. Concurrently, the plagioclase feldspars display complex zoning but an overall trend of decreasing An-content with differentiation. Mineral reactions in olivine and the Fe - Ti oxide phases indicate equilibration under conditions which may be reconciled with sustained high temperature oxidising conditions probably due to the contemporaneity of large volumes of cooler, volatile rich, acid magma (Gamble, 1979b).

ACKNOWLEDGEMENTS

I thank Robin Offler, Paul Lyle, Ian Meighan and Jack Preston for careful reviews and helpful comments. The paper has benefitted from discussions with Dave French, Rodney Grapes, Chris Baker, Jim Cole and many other colleagues. Electron microprobe analyses were carried out in the Electron Microscope Facility of Newcastle University, N.S.W., Australia. Gordon Johnston and Nick Ware (A.N.U.) are thanked for their assistance. The material was collected during the tenure of research scholarships from the Ministry of Education, N. Ireland and the Queen's University of Belfast. I thank Danuta Winterborn and Val Hibbert for typing drafts of the manuscript and Jan Barnes and Mark Phillips for assistance with photography and drafting of diagrams.

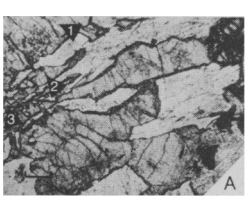

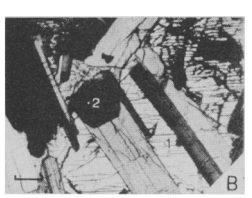

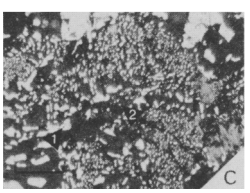

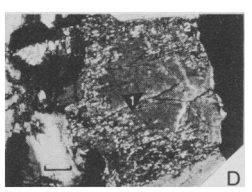

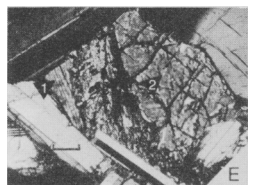

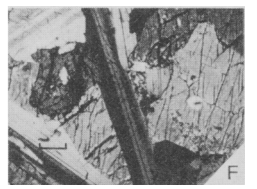

Photomicrographs A-F of textural relationships in dolerites and gabbros from the Slieve Gullion central complex. Bar represents 0.1mm. Numbers refer to electron microprobe analyses which are contained in the Appendix.

Plate 1A, specimen AT1490, subvariolitic crystallisation of clinopyroxene (augite) and plagioclase.

Plate 1B, specimen 72/41, clinopyroxene (augite) and plagioclase showing ophitic texture.

Plate 1C, specimen 72/24, magnetite-orthopyroxene symplectite formed by oxidation of olivine.

Plate 1D, specimen AT40, complex clinopyroxene grain, an optically homogenous core (analyses D1) is surrounded by a zone of amphibole intergrowth. The outer rim of the grain is mantled by a later overgrowth of clinopyroxene (analysis D2).

Plate 1E, specimen 72/41, olivine (analysis E2) with marginal pigeonite (inverted to orthopyroxene with associated complex exsolution). Augite (analysis E1) has grown parallel to pigeonite.

Plate 1F, specimen 72/41, ophitic crystallisation involving clinopyroxene (augite) and plagioclase.

APPENDIX

Electron microprobe analyses of minerals at the points illustrated in Plate 1A-F. cpx: Ca-rich pyroxene; opx: Ca-poor pyroxene; mt: magnetite.

Plate number, specimen and analysis number	PLATE 1A AT1490 A1	PLATE 1A AT1490 A2	PLATE 1A AT1490 A3	PLATE 1B 72/41 B1	PLATE 1B 72/41 B2
Mineral analysed element oxide	cpx	cpx	cpx	cpx	olivine
SiO_2	52.94	52.20	51.74	51.71	36.08
TiO_2	0.27	0.45	0.66	0.78	-
Al_2O_3	1.83	2.03	3.00	2.27	-
FeO*	8.68	9.41	9.16	8.48	27.46
MnO	0.20	0.21	0.31	0.32	0.38
MgO	15.86	14.34	15.85	14.19	36.08
CaO	19.65	20.67	18.58	21.94	-
Na_2O	0.31	0.42	0.45	0.31	-
Cr_2O_3	0.13	0.26	0.25	0.20	-
Total	99.87	99.99	100.00	100.20	100.00

	PLATE 1C 72/24 C1 opx	PLATE 1C 72/24 C2 mt	PLATE 1D AT40 D1 cpx(core)	PLATE 1D AT40 D2 cpx(rim)	PLATE 1E 72/41 E1 cpx(rim)	PLATE 1E 72/41 E2 olivine
SiO_2	49.96	0.24	52.52	52.42	51.05	36.94
TiO_2	0.45	2.94	0.51	0.24	0.94	-
Al_2O_3	1.35	1.32	1.78	0.50	2.05	0.27
FeO*	25.39	89.08	10.17	12.64	12.65	27.83
MnO	0.96	0.16	0.25	0.43	0.33	0.64
MgO	20.31	-	15.51	12.35	15.33	34.03
CaO	0.93	-	19.00	20.94	17.38	-
$Na_2O(V_2O_3)$*	-	0.97	0.25	0.49	0.57	-
Cr_2O_3	0.21	0.34	-	-	-	-
Total	99.56	95.05	99.99	100.01	99.99	99.77

+ Total iron as FeO

* V_2O_3 in mt. analysis

REFERENCES

Anderson (A.T.), 1976. J. Volc. Geotherm. Res. 1, 3 - 33.

Bailey (E.B.) and McCallien (W.J.), 1956. Lpool. Manchr. Geol. J. 1, p. 466.

Bence (A.E.) and Papike (J.J.), 1972. Proc. Lunar Sci. Conf., 3rd. 1, 431 - 468.

Bowles (J.F.W.), 1977. Mineral. Mag. 41, 103 - 109.

Buddington (A.F.) and Lindsley (D.H.), 1964. J. Petrol. 5, 310 - 357.

Carmichael (I.S.E.), 1967. Contrib. Mineral. Petrol. 14, 36 - 64.

Coish (R.A.) and Taylor (L.A.), 1979. Earth, Planet. Sci. Letts. 42, 389 - 398.

Coleman (L.C.), 1976. Contrib. Mineral. Petrol. 66, 221 - 227.

Cook (A.H.) and Murphy (T.), 1952. Dubl. Inst. Adv. Studies, Geophys. Mem. No. 2, 4, 1 - 35.

Deer (W.A.) and Abbott (D.), 1965. Mineral. Mag. 34, 177 - 193.

Deer (W.A.), Howie (R.A.) and Zussman (J.), 1978. Rock Forming Minerals, Vol. 2A: Single-chain silicates. 2nd Ed. Pub. Longmans.

Donaldson (C.H.), 1977. J. Petrol. 18, 595 - 620.

Drever (H.I.) and Johnston (R.), 1966. J. Petrol. 7, 414 - 420.

Dunham (A.C.) and Wadsworth (W.J.), 1978. Mineral. Mag. 42, 347 - 356.

Eichelberger (J.C.), 1980. Nature 288, 446 - 450.

Elsdon (R.), 1971. Mineral. Mag. 38, 49 - 57.

Emeleus (C.H.), 1962. Proc. R. Ir. Acad. (B) 62, 55 - 76.

Esson (J.), Dunham (A.C.) and Thompson (R.N.), 1975. J. Petrol. 16, 488 - 497.

Gamble (J.A.), 1975. Unpub. Ph.D. thesis, The Queen's University, Belfast.

Gamble (J.A.), 1979a. Contrib. Mineral. Petrol. 69, 5 - 19.

Gamble (J.A.), 1979b. J. Volc. Geotherm. Res. 5, 297 - 316.

Gamble (J.A.), Old (R.A.) and Preston (J.), 1976. Rep. Inst. Geol. Sci. No. 76/8, 17 pp.

Gibb (F.G.F.), 1976. J. Geol. Soc. London 132, 209 - 222.

Grove (T.L.) and Bence (A.E.), 1977. Proc. Lunar Sci. Conf. 8th. 2, 1549 - 1579.

Haggerty (S.E.) and Baker (I.), 1967. Contrib. Mineral. Petrol. 16, 233 - 257.

Himmelberg (G.R.) and Ford (A.B.), 1977. Am. Mineral. 62, 623 - 633.

Huebner (J.S.), Ross (M.) and Hickling (N.), 1975. Proc. Lunar Sci. Conf. 6th, 529 - 546.

Johannes (W.), 1978. Contr. Mineral. Petrol. 66, 295 - 303.

Mattey (D.P.), Gibson (I.L.), Marriner (G.F.) and Thompson (R.N.), 1977. Mineral. Mag. 41, 273 - 285.

Mevel (C.) and Velde (D.), 1976. Earth. Planet. Sci. Letts. 32, 158 - 164.

Nobugai (K.), Tokonami (M.) and Morimoto (N.), 1978. Contrib. Mineral. Petrol. 67, 111 - 118.

Nwe (Y.Y.), 1976. Contrib. Mineral. Petrol. 55, 105 - 126.

Papike (J.J.), Cameron (K.L.) and Baldwin (K.), 1974. Geol. Soc. Am. Abst. Prog. 6, 1053 - 1054 (abst.).

Putnis (A.), 1976. Mineral. Mag. 43, 293 - 296.

Reed (S.J.B.) and Ware (N.G.), 1975. J. Petrol. 16, 499 - 519.

Reynolds (D.L.), 1951. Trans. Roy. Soc. Edin. 62, 85 - 147.

Richey (J.E.) and Thomas (H.H.), 1932. Quart. J. Geol. Soc. London 88, 766 - 849.

Richey (J.E.), 1935. Proc. Geol. Assoc. 46, 487 - 492.

Ross (M.) and Huebner (J.S.), 1975. Extd. Abstr., Penn. State Univ. 4 pp.

Ross (M.), Huebner (J.S.) and Hickling (N.), 1973. Proc. Lunar Sci. Conf. 637 - 639.

Sparks (S.R.J.), Sigurdsson (H.) and Wilson (L.), 1977. Nature 267, 315 - 318.

Thompson (R.N.), Esson (J.) and Dunham (A.C.), 1972. J. Petrol. 13, 219 - 254.

Thompson (R.N.), Gibson (I.L.), Marriner (G.F.), Mattey (D.P.) and Morrison (M.A.), 1980. J. Petrol. 21, 265 - 294.

Wager (L.R.) and Brown (G.M.), 1968. Layered Igneous Rocks. Edinburgh and London: Pub. Oliver and Boyd.

Wells (P.R.A.), 1977. Contrib. Mineral. Petrol. 62, 129 - 140.

Wood (B.J.) and Banno (S.), 1973. Contrib. Mineral. Petrol. 42, 109 - 124.